Advanced Steel Construction – Vol. 18 No. 4 (2022) 818–825
DOI:10.18057/IJASC.2022.18.4.9

EXPERIMENTAL STUDIES OF THE SORBITE STAINLESS STEEL PLUG-PIN SCAFFOLD JOINT

Nan Xie [1], Tao Du [1,*], Fei-Fei Qin [2] and Peng-Sheng Geng [3]

[1] *School of Civil Engineering, Beijing Jiaotong University, Beijing 100044, China*
[2] *Cost Management Department, Zhongliang Holdings Group Shandong Regional, Jinan 250000, China*
[3] *Engineering Department, China LVFA Investment Group Shandong Regional, Qingdao 266000, China*
** (Corresponding author: E-mail: dutao347@sina.com)*

ABSTRACT

Systematic experimental studies were performed for the purpose of obtaining the material properties of cold-formed sorbite stainless steel and the mechanical parameters of plug-pin joint. As a new type of material, the scaffold made of sorbite stainless steel has the advantages of convenient construction, high strength and stainless steel. The static tensile tests for S500 sorbite stainless steel investigating the material characteristics of plug-pin joint were carried out. The bending moment, the compressive force, the tensile force and the shear force were applied to the joint respectively. To get the failure modes and moment-rotation (or load-displacement) curves, the joint behavior, including the semi-rigidity between the ledger and the standard, compression and shear of the standard, and the tension of the ledger joint were studied. The result can determine the load-bearing capacity and the performance of the joint. The joint stiffness was determined according to different methods and four models were proposed to describe the bending behavior. By analyzing the different modes of joint failure, the weak part can be determined to provide basis for actual joint design.

ARTICLE HISTORY

Received: 13 April 2022
Revised: 20 May 2022
Accepted: 22 May 2022

KEYWORDS

Sorbite stainless steel;
Plug-pin joint;
Bending model;
Stiffness;
Strength

1. Introduction

Scaffold system is a temporary structure commonly used to support workers, materials and buildings during construction. Recently, many scaffold collapse accidents have occurred all over the world, which may not only cause project delay but also lead to a large number of casualties [1, 2]. The scaffold collapse occurred at a construction site in China as shown in Fig. 1. Therefore, the safety of scaffold system is more and more widely concerned.

Fig. 1 Scaffold collapse at a construction site in China

The behavior of joint has significant effects on the overall properties of scaffold system. It is necessary to deeply study the mechanical behavior of scaffold joint. The behavior of joint is complex, mainly due to the rapid assembly of scaffold system in construction and the connection of components at different angles. The joints are the weakest components in the scaffold system, and structural components are less likely to be damaged than the connections between joints [3, 4]. In the scaffold system, since the joint plays the role of connecting the standard, ledger and brace and the mechanical behavior of the joint is not rigid or hinge but semi-rigid, the stiffness of the joint has a significant impact on the bearing capacity of the scaffold system [5-8]. Therefore, in order to avoid the collapse of scaffold system, it is necessary to analyze the connection characteristics of joints in detail. Laboratory tests and numerical simulations are the important ways to obtain the mechanical properties of the joints.

It is the most important problem to determine performance of the joints for studying the bearing capacity of scaffold system. There are many types of scaffold joints, including coupler joints, cuplock joints, mortise-tenon joints and wedge joints, etc. Many researchers have done a lot of research on them and achieved significant results. Jia et al. [9] conducted experimental research on the slip stiffness and rotational stiffness of right-angle coupler joints, and obtained the failure modes. Several tests have been conducted on the performance of couplers under cyclical loads, and obtained the influence of looseness on the bearing capacity through tests and calculations [10-12]. Chandrangsu and Rasmussen [13] performed experiments on the behavior of coplock joints and proposed to use the trilinear moment-rotation curve to describe the stiffness of the joints. For a mortise-tenon joint, a series of frame experiments were carried out. The results showed that compared with the fastener scaffold, the mortise-tenon scaffold had significant advantages in the mechanical properties of the joints and the bearing capacity of the frame [14]. Peng et al. [15] investigated the effects of different parameters such as number of stories, ground heights and joint positions on the behavior of spigot joints, and determined the corresponding joint stiffness. Bong et al. [16] conducted tests on the repeatedly used wedge joints, and obtained initial stiffness by probability analysis. The experiments were carried out on the ringlock joints under different forms of forces, and the behavior and the load-bearing capacity were obtained [17]. Zhao et al. [18] and Dong et al. [19] studied the mechanical properties of socket joints and the overall performance for the scaffold by tests and finite element numerical analysis. Chen and Zhao [20] proposed a new numerical method that can be used in analysis of joint stiffness, and discussed the influence of splice joint stiffness on the ultimate bearing capacity of modular scaffold. Liu et al. [21] investigated the mechanical performance of the plug-pin joints based on the visual system, and obtained the joint stiffness corresponding to different forms of loads by fitting method. As a new type of material, the scaffold made of sorbite stainless steel has the advantages of convenient construction, high strength and stainless steel. At present, there is little research on the behavior of plug-pin joints made of sorbite stainless steel, which are widely used to build temporary stands and stages.

In this paper, the mechanical behavior of sorbite stainless steel plug-pin joints (Fig. 2) was comprehensively studied with experiments. The S500 sorbite stainless steel material used in this study was 12Cr14Ni2 [22]. The properties of the new material used to make joint components were obtained by the static tensile tests. Tests were performed on the joints under different forms of loads, including bending moment, tension, compression and shear force, to determine the connection performance and load-bearing capacity. Moreover, the weak part in the plug-pin joint was determined.

2. Material test of sorbite stainless steel

For the plug-pin joints, except that the wedge is made of cast iron, and the rest are made of sorbite stainless steel. In order to obtain the material properties

of sorbite stainless steel made into the main joint components, static tensile tests were carried out on 8 groups of specimens. A 25cm long pipe section was cut from a batch of the joint element. Two arc specimens were cut longitudinally at 90° positions on both sides of the weld. Schematic diagram of the specimen is shown in Fig. 3. Vernier caliper was used to measure the dimensions of each test specimen. The statistical results are shown in Table 1. After the specimens were measured, a strain gauge was pasted at the center point of concave and convex of each longitudinal arc specimen (Fig. 4).

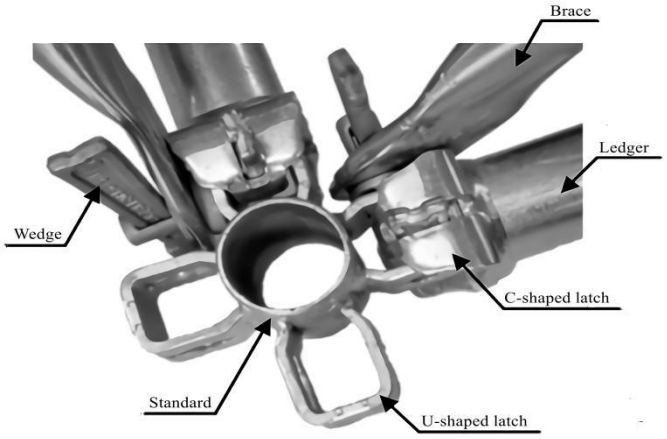

Fig. 2 Components of a plug-pin joint

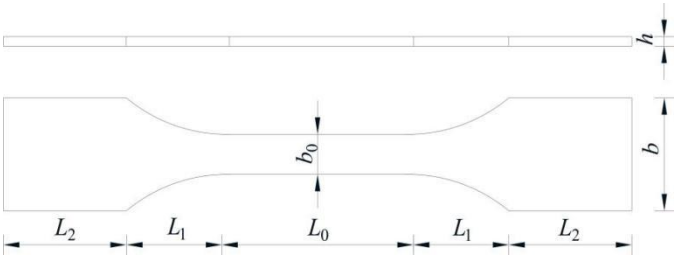

Fig. 3 The schematic diagram of specimen

Table 1
Measured dimensions of specimens

Specimen NO.	Dimensions (mm)					
	b_0	L_0	L_1	L_2	L	h
T48-1	10.1	50.1	25.6	40.9	157.4	2.4
T48-2	10.3	50.4	25.6	40.6	157.1	2.2
T48-3	10.0	50.0	25.4	40.9	157.1	2.3
T48-4	10.1	50.4	25.5	40.7	157.3	2.3
T48-5	10.1	50.5	25.5	40.7	157.3	2.4
T48-6	10.2	50.1	25.6	40.8	157.3	2.5
T48-7	10.1	50.5	25.5	40.6	157.1	2.4
T48-8	9.9	50.3	25.4	40.8	157.3	2.4

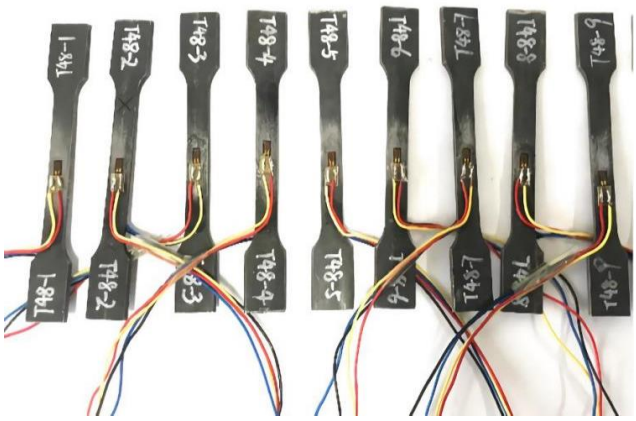

Fig. 4 Specimens with strain gauges

The equipment used for loading was WAW200 microcomputer controlled electro-hydraulic servo universal testing machine. Before the strain reached 2%, the loading rate was 0.2mm/min. When the strain reached 2%, the deformation rate accelerated with the increase of tensile force. The loading rate was changed to 0.5mm/min until the specimen was failure. Fig. 5 presents the tensile test setup before loading.

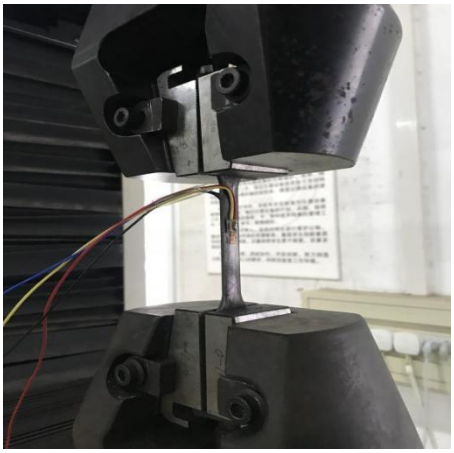

Fig. 5 Tensile test setup

Eight stress-strain curves and corresponding average curve were obtained through the tests (Fig. 6). As seen, a nonlinear stress-strain relationship was observed. As the strain increased, the slope of the curve decreased gradually. After the strain gauge fell off, the stress still continued to increase, indicating that the material has obvious strain hardening. The test results of material properties for specimens are presented in Table 2. Where, E is the elastic modulus, f_y is the yield strength, f_u is the ultimate strength.

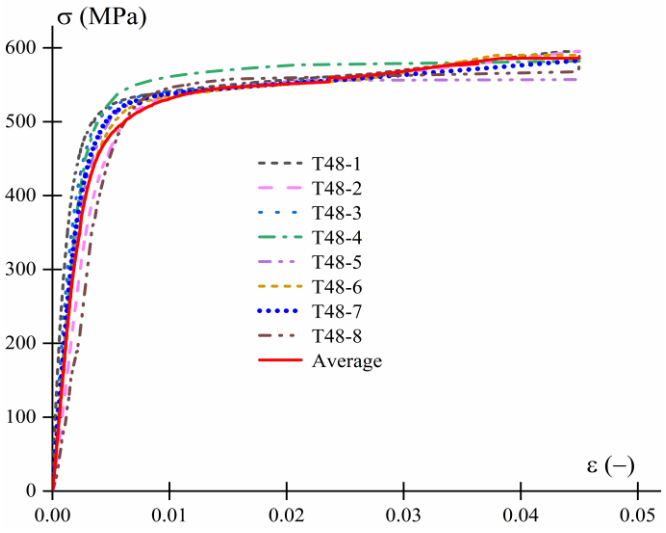

Fig. 6 Stress-strain characteristics of the material

Table 2
Material characteristics of sorbite stainless steel

Specimen NO.	E (GPa)	f_y (MPa)	f_u (MPa)
T48-1	194	509	594
T48-2	197	491	596
T48-3	181	510	585
T48-4	189	530	582
T48-5	178	499	552
T48-6	207	495	589
T48-7	206	509	583
T48-8	197	518	600
Average	194	508	585

3. Test of joint

The plug-pin joint is mainly composed of C-shaped latch, U-shaped latch and wedge. A C-shaped latch is welded to the ledger end, which has upper and lower sockets. The U-shaped latch is welded on the surface of the standard. And the wedge is a steel plate part used to connect the C-shaped latch to the U-shaped latch. The detailed dimensions of these main elements are shown in Fig. 7.

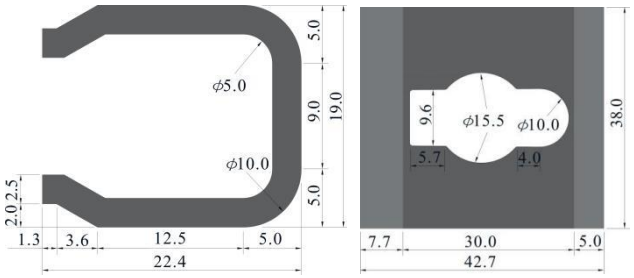

(a) U-shaped latch

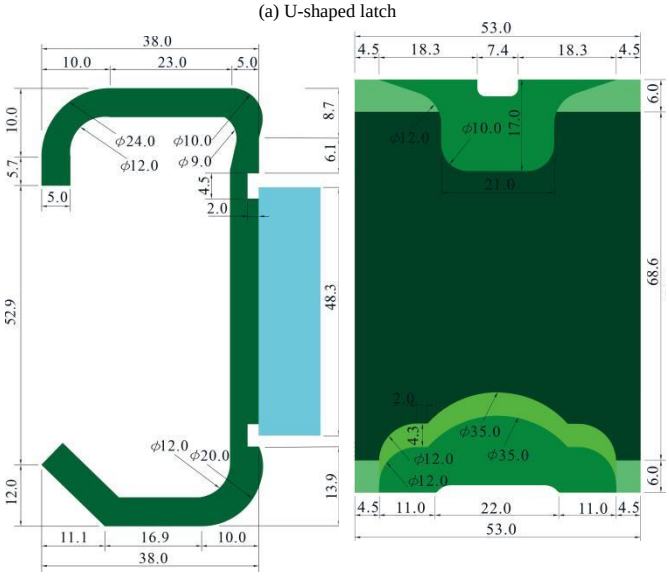

(b) C-shaped latch

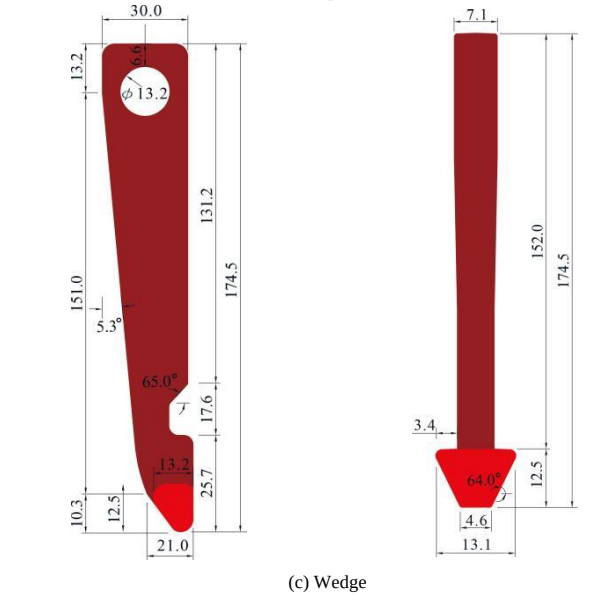

(c) Wedge

Fig. 7 The detailed dimensions of the main elements (mm)

The plug-pin joint was tested under different forms of loads including bending moment, tension, compression and shear force. The circular section size of the standard and the ledger pipe is Φ48.3 mm×2.2 mm. The samples adopted in each test were the same material that have not been used. Tests were carried out under displacement control until the specimen was failure or the force increased no more.

3.1. Joint bending test

Positive and negative bending tests were conducted on plug-pin joints to obtain the rotational performance. Firstly, the lower end of the standard was fixed with the support. Secondly, fixing the support with the testing machine by M12 high-strength bolts. Finally, the pressure head of the testing machine was pressed on the ledger. The rotational stiffness between standard and ledger varies with the rotational direction. For positive bending test (Fig. 8(a)), the bending moment M_P was generated by applying force F_P on the ledger. For negative bending test (Fig. 8(b)), the bending moment M_N was generated by applying force F_N on the ledger.

In order to measure the rotation angle, four Linear Variable Differential Transformers (LVDTs) were adopted to measure the displacement of standard and ledger in the test. The schematics of the load and LVDTs arrangement for the positive and negative bending tests are given in Figs. 8(c) and 8(d). Displacement controlled loading was adopted in the tests, and the loading rate was 0.5 mm/min. Preloading was carried out before the test began.

(a) Test setup of positive bending

(b) Test setup of negative bending

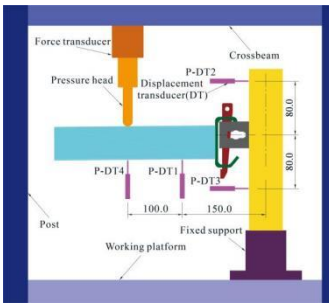

(c) Layout of LVDTs for positive bending

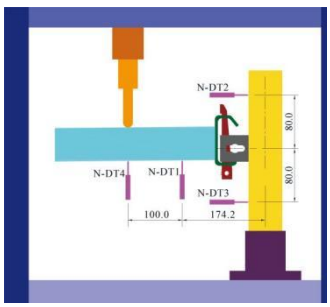

(d) Layout of LVDTs for negative bending

Fig. 8 Bending test configuration and LVDTs locations (mm)

The calculation formula for the positive bending moment M_P is given by

$$M_P = F_P L_P \tag{1}$$

Where F_P is the vertical concentrated load at the loading point of the ledger, and L_P =250.0 mm is the distance from the loading point to the standard pipe center.

The calculation formula for the negative bending moment M_N is given by

$$M_N = F_N L_N \tag{2}$$

Where F_N is the vertical concentrated load at the loading point of the ledger, and L_N =374.2 mm is the distance from the loading point to the standard pipe center.

The formula for calculating the rotation angle θ can be determined as follows

$$\theta = \arctan\left(\frac{\Delta_4 - \Delta_1}{d_{14}}\right) - \arctan\left(\frac{\Delta_2 - \Delta_3}{d_{23}}\right) \tag{3}$$

Where for positive bending test, Δ_1, Δ_2, Δ_3, Δ_4 are the displacements of transducers P-DT1 to P-DT4, d_{14} is the distance between transducers P-DT1 and P-DT4, and d_{23} is the distance between transducers P-DT2 and P-DT3; for negative bending test, Δ_1, Δ_2, Δ_3, Δ_4 are the displacements of transducers N-DT1

to N-DT4, d_{14} is the distance between transducers N-DT1 and N-DT4, and d_{23} is the distance between transducers N-DT2 and N-DT3.

According to Equation (1), Equation (2) and Equation (3), the bending moment M of each test and its corresponding rotation angle θ were obtained, from which the M-θ curve can be drawn.

Two failure modes occurred in the positive bending test (Fig. 9) and one failure mode occurred in the negative bending test (Fig. 10). As shown in Fig. 9(a), the joint failure mode I in the positive bending test was that the C-shaped latch at the contact position with the wedge. The fracture occurred in the C-shaped latch and the wedge presented obvious plastic deformation at the contact areas. The fracture of C-shaped latch is mainly because the C-shaped latch is formed by cold bending of sorbite stainless steel plate, and it is relatively weak in the cold bending position. As shown in Fig 9(b), the joint failure mode II in the positive bending test was that the surface of the standard at the lower edge of the U-shaped latch was squeezed and concave by the C-shaped latch and the lower edge of the U-shaped latch presented obvious plastic deformation at the contact position. The concave surface occurred is mainly because the stress point changes after the C-shaped latch contacts standard pipe surface, and the contact position of the standard becomes the main stress point. Among the nine groups of specimens, KW48-2 belonged to failure mode II, and the rest belonged to failure mode I. The failure mode was the wedge buckling, which was obvious for the negative bending test (Fig. 10). No significant change was observed in the weld area connecting the U-shaped latch and the standard in both the positive bending test and the negative bending test.

(a) Failure mode I

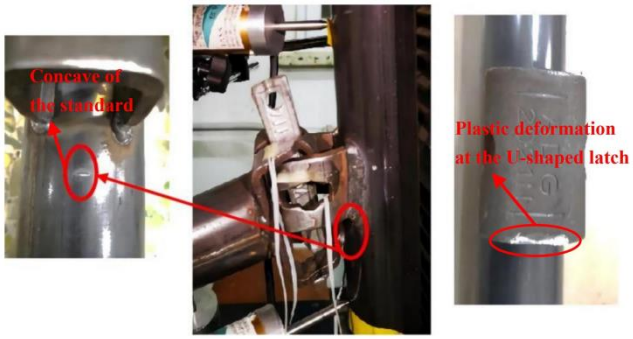

(b) Failure mode II

Fig. 9 Failure behavior after positive bending test

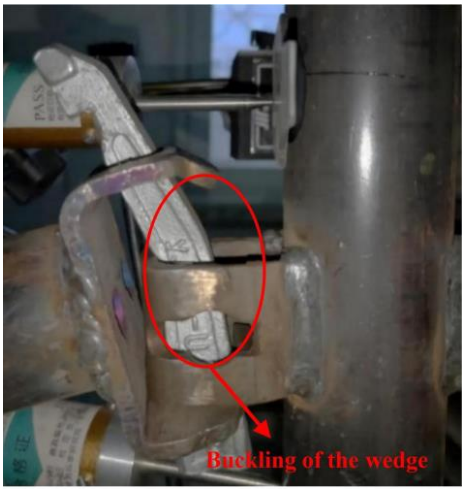

Fig. 10 Failure behavior after negative bending test

According to nine groups of bending test results, the bending moment-rotation curves and the average curve of the joint were obtained (Fig. 11). As can be seen from Fig. 11, the plug-pin joint has non-linear moment- rotation curves. Because of the asymmetrical nature, the plug-pin joint presents different behaviour under positive and negative rotations. The ultimate bearing capacity and rotational stiffness of the positive bending are greater than those of the negative bending.

3.2. Joint tensile test

The tensile test was performed to obtain the tensile performance and failure mode. In order to smoothly conduct the test, two steel bars with a diameter of 16 mm instead of the ledgers were welded on the C-shaped latches (Fig. 12). The constant displacement of each test was increased by 0.5 mm/min until the specimen was completely damaged. Preloading was carried out before the test began.

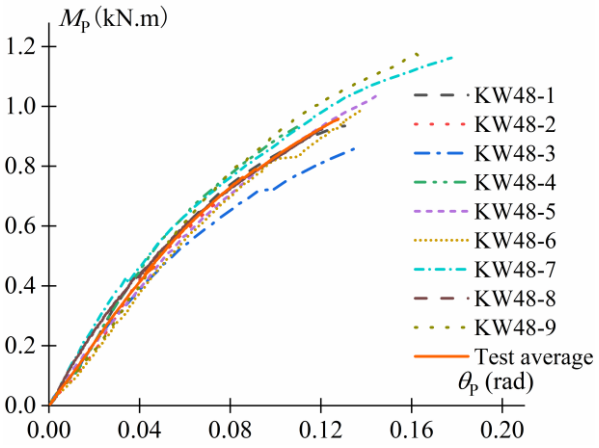

(a) Moment-rotation curves for positive bending test

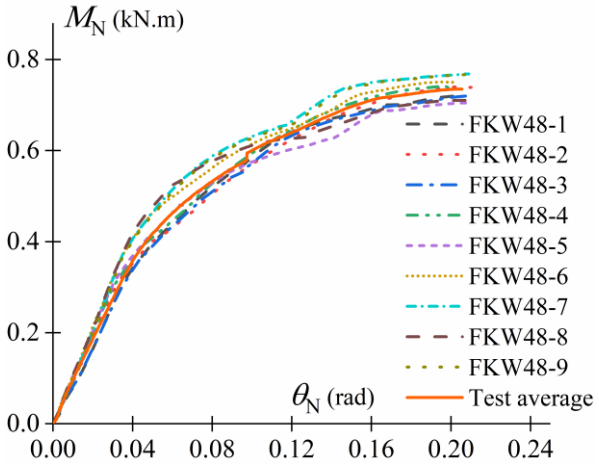

(b) Moment-rotation curves for negative bending test

Fig. 11 Moment-rotation curves for bending test

(a) Tensile test setup

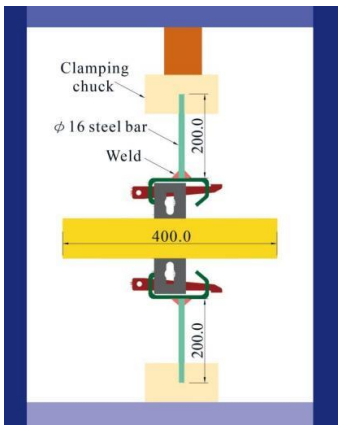

(b) Tensile test scheme

Fig. 12 Tensile test configuration (mm)

Six groups of tensile tests were carried out. The failure mode of the plug-pin joint was at the contact position between the C-shaped latch and the wedge (Fig. 13). The fracture occurred in the upper bending part of the C-shaped latch (Fig. 13(a)). There were two failure modes of the wedge. The wedge for KL48-2, KL48-3 and KL48-5 was bending and torsional failure (Fig. 13(b)), while for other specimens were pure bending failure (Fig. 13(c)). The installation without centered and defects of the wedge lead to bending and torsional failure. The specimen of each tensile test was observed to be brittle failure. Therefore, the upper bending part of the C-shaped latch needs to be improved in the design.

(a) Fracture at the C-shaped latch

(b) Bending and torsional failure of the wedge

(c) Pure bending failure of the wedge

Fig. 13 Failure behavior after tensile test

Based on the tensile test results, the load-displacement F_T-d_T curves and the average curve of the joint can be obtained (Fig. 14). As can be seen from Fig. 14, the maximum load of the specimens including KL48-2, KL48-3, KL48-5 is obviously less than that of other specimens. In order to avoid the bending and torsional failure of the wedge, the wedge should be installed correctly and checked whether the material is qualified in practical applications.

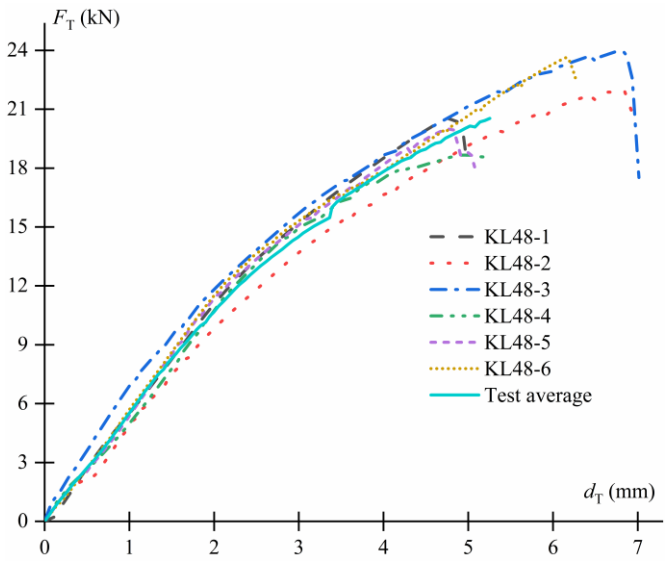

Fig. 14 Load-displacement curve for tensile test

3.3. Joint compressive test

The compressive test was performed to obtain the compressive performance and failure mode of the joint. Each end of the standard was respectively covered with a support, and the wedge was inserted tightly (Fig. 15). The constant displacement of each test was increased by 0.5 mm/min, until the force increased no more. Preloading was carried out before the test began.

Three groups of compressive tests were carried out. The failure mode of the plug-pin joint was that the standard was observed to have obvious depression. The standard showed buckling and there was no obvious deformation in other positions of the joint (Fig. 16).

According to test results, the load-displacement F_C-d_C curves and the average curve of the joint are plotted (Fig. 17). As shown in Fig. 17, the experimental results are discrete. After measurement, the main reason is that the U-shaped latches on both sides are not welded in a straight line with the standard.

(a) Compressive test setup

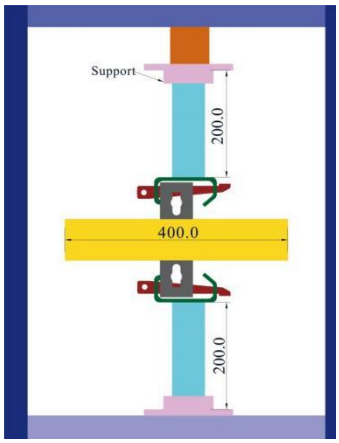

(b) Compressive test scheme

Fig. 15 Compressive test configuration (mm)

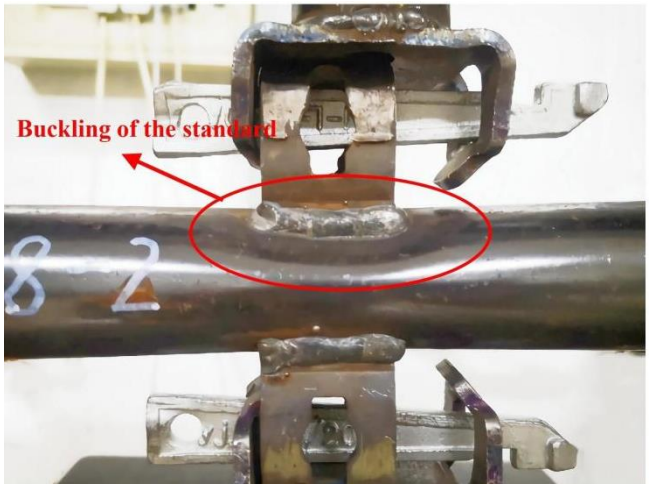

Fig. 16 Failure behavior after compressive test

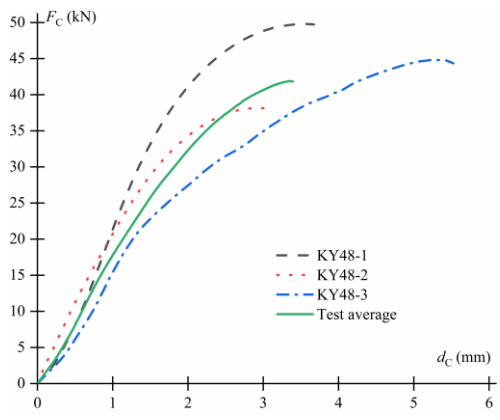

Fig. 17 Load-displacement curve for compressive test

3.4. Joint shear test

The shear test was conducted to obtain the shear performance and failure mode of the joint. Two cylindrical iron blocks were placed on both sides of the specimen. A steel base plate is placed on the upper part of the iron block, and a support was placed on the top of the standard (Fig. 18). According to different shear methods, the shear test included the internal and external shear test. The internal shear test refers to placing the iron blocks and steel base plates on both sides close to the surface of the standard. The schematics of setup and loading scheme for the internal shear test are given in Figs. 18(a) and 18(b). The external shear test refers to placing both sides of the iron blocks and steel base plates at 7 mm away from the lower edge of the U-shaped latches. The schematics of setup and loading scheme for the external shear test are presented in Figs. 18(c) and 18(d). The constant displacement of each test was increased by 1 mm/min until the force increased no more. Preloading was carried out before the test began.

(a) Internal shear test setup

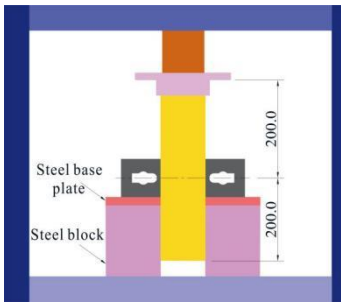

(b) Internal shear test scheme

(c) External shear test setup

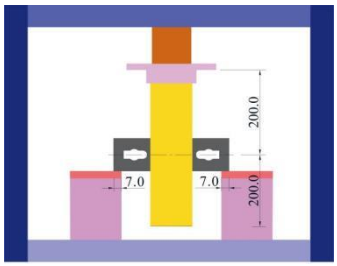

(d) External shear test scheme

Fig. 18 Shear test configuration (mm)

The failure modes are presented in Fig. 19. For the internal shear test, the failure modes were the extrusion deformation of the standard and the obvious deformation of the U-shaped latches (Fig. 19(a)). For the external shear test, the failure modes were weld cracking at the connection and the extrusion deformation of the standard (Fig. 19(b)).

(a) Failure mode of internal shear test

(b) Failure mode of external shear test

Fig. 19 Failure behavior after shear test

According to test results, the load-displacement curves and the average curve are plotted (Fig. 20).

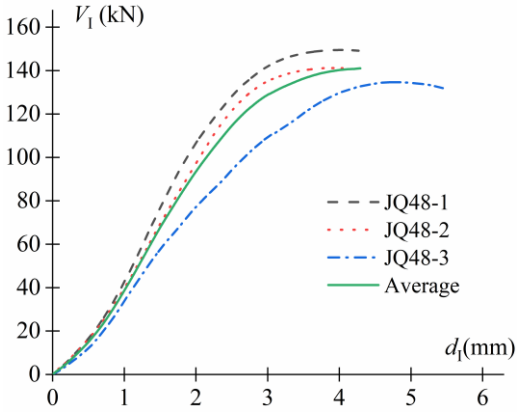

(a) Load-displacement curve for internal shear test

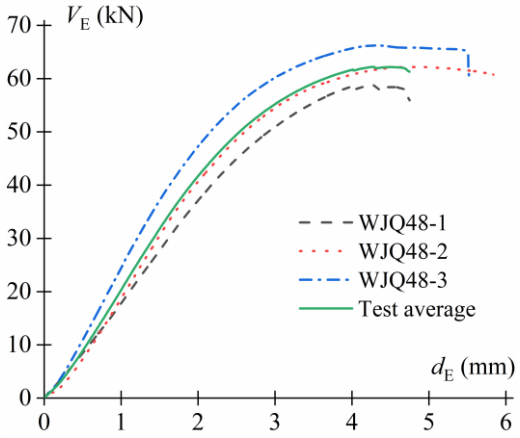

(b) Load-displacement curve for external shear test

Fig. 20 Load-displacement curve for shear test

4. Load bearing capacity and bending models

After determining the moment-rotation curves and load-displacement curves from the test results, Eurocode EN 12811-3:2002 [23] can be adopted to predict the load bearing capacity of plug-pin joint. Eurocode EN 12811-3:2002 [23] specifies the rules for the evaluation of test results in the field of temporary works. For the scaffold joint, due to the repeated use of the components, it is unacceptable if irreparable damage occurs. The bearing capacity of the joint is determined from the limit imposed by Eurocode EN 12811-3[23] on the ultimate load value. Under this restriction, it is ensured that the joint mainly works within the linear-elastic range. Therefore, the possibility of plasticity can be limited by reducing the ultimate load value measured in the test. According to the nominal characteristic value $R_{k,norm}$ predicted in EN12811-3:2002 [23], this value is the maximum allowable strength value namely the load bearing capacity [12]. The nominal characteri- stic value $R_{k,norm}$ is determined as follows:

$$R_{k,norm} = \frac{R_{k,b}}{\gamma_{R,2}} \tag{4}$$

Where $R_{k,b}$ is the basic characteristic value of resistance, γ_{R2} is the partial safety factor depending on the ductility. The value of γ_{R2} is determined as follows:

$$1.25 \geq \gamma_{R2} = -0.025\overline{q_e} + 1.275 \geq 1.0 \tag{5}$$

Where is $\overline{q_e}$ the mean value of plastic and elastic energy quotient [23].

Based on the experimental results and Eurocode, the load bearing capacity of the plug-pin joint under corresponding loads can be obtained by combining Equation (4) with Equation (5), as indicated in Table 3.

The rotational behavior of the joint has significant effects on overall performance of the scaffold structure. The structure tends to bend and damage in

the direction parallel or perpendicular to the elevation of the joint [8]. The rotational behavior is expressed via the instantaneous rotational stiffness. It is necessary to develop the bending model of the joint for the establishment of the numerical model. Due to the asymmetry, in the case of positive rotation and negative rotation, the behavior of joint is usually different. Therefore, based on the bending test results, this paper developed the bending model of the joint in the vertical plane for the positive and negative rotation.

Table 3
Load bearing capacity of the plug-pin joint

Load forms	Basic characteristic value	Load bearing capac-
Positive bending moment	0.85 kN.m	0.82 kN.m
Negative bending moment	0.68 kN.m	0.64 kN.m
Tensile force F_T	20.53 kN	17.70 kN
Compression force F_C	38.16 kN	35.98 kN
Internal shear force V_I	128.97 kN	121.63 kN
External shear force V_E	56.13 kN	52.88 kN

Four methods were used to obtain nonlinear bending models within the load range related to the characteristic value $R_{k,norm}$. The first method was a bilinear curve obtained according to SEMA code [24]. The initial stiffness value was the slope determined by the line between the original point and the point from the test curve at maximum bending moment. When the rotation was greater than that determined by the maximum bending moment point at the initial line, the moment remained unchanged. The second method was a bilinear curve obtained according to the initial stiffness value and maximum bending moment, assuming that the initial stiffness value resulting from the tangent slope of the test curve. The initial line was defined by approximate the tangent of the test curve at original point. The linear function was used to simulate the tangent passing through the zero load point. The bilinear curve was called the initial stiffness curve. The third method was the equal area approach proposed in Eurocode EN 1551- 2:2009 [25]. This method was originally developed based on the Federation Europeenne de la Manutention (FEM) to model the behavior of pallet racks. Because the mechanical proper- ties of scaffold and pallet structure are similar, this method is considered to be a suitable method to simulate the bending model of joint. The initial stiffness value was the slope of the line passing through the origin point, which divided the test curve below the maximum bending moment into two parts. Finally, the area of the two parts was kept equal. The last method was to obtain trilinear curves by fitting the test data in the range of maximum bending moment. The simple polynomial function was used to simulate the experim- ental curve in order to provide the best fitting for the test data. The polynomial function was derived by approximating the test result.

The model was developed by using simple expressions. Fig. 21 shows the test curve for the positive and negative rotation and the approximate bending model obtained by four methods. The mathematical expressions corresponding to the four bending models are given in Table 4.

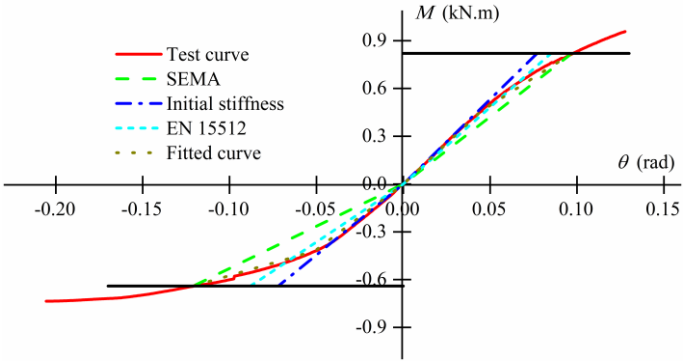

Fig. 21 Joint bending models

5. Conclusions

In this paper, the material properties of cold formed sorbite stainless steel and the mechanical behavior of the plug-pin joint made of cold formed sorbite stainless steel were studied. The results can provide material properties and mechanical parameters for developing numerical models of the joint, which can determine the load bearing capacity and weak parts under different forms of loads. The following conclusions can be obtained:

The material properties of sorbite stainless steel has nonlinear stress- strain relationship and obvious strain hardening phenomenon.

The failure modes of the joint under tensile force was brittle failure. The upper bending part of the C-shaped latch needs to be improved in the design. The plug-pin joint had different failure modes under various forms of loads, which can provide reference for practical design and analysis. The ultimate bearing capacity and rotational stiffness of the positive bending are greater than those of the negative bending. Four methods were adopted to build the bending model within the range of load bearing capacity. It can provide enough mechanical parameters for the refined numerical model established by the three-dimensional nonlinear analysis of the structure, which can also provide a reference for the stability calculation of the overall structure.

Based on the test results, the weak part is the upper bending position of the C-shaped latch, which can greatly affect the bearing capacity of the joint under different forms of load. Therefore, the the upper bending position of the C-shaped latch should be optimized in the design of the plug-pin joint. However, the influence of the reuse and welding residual stress on the mechanical behavior for joint were not considered in this work. In the future research, the two aspects will be further studied and the conclusion will be improved.

Table 4
Four bending models for the plug-pin joint

Model	Positive bending		Negative bending	
	Rotation (rad)	Expressions	Rotation (rad)	Expressions
SEMA	$0\leq\theta_P<0.097$	$M_P=8.45\theta_P$	$-0.121\leq\theta_N<0$	$M_N=5.33\theta_N$
	$\theta_P\geq0.097$	$M_P=0.82$	$\theta_N<-0.121$	$M_N=-0.64$
Initial stiffness	$0\leq\theta_P<0.077$	$M_P=10.61\theta_P$	$-0.072\leq\theta_N<0$	$M_N=8.92\theta_N$
	$\theta_P\geq0.077$	$M_P=0.82$	$\theta_N<-0.072$	$M_N=-0.64$
EN 15512	$0\leq\theta_P<0.085$	$M_P=9.65\theta_P$	$-0.088\leq\theta_N<0$	$M_N=7.27\theta_N$
	$\theta_P\geq0.085$	$M_P=0.82$	$\theta_N<-0.088$	$M_N=-0.64$
Fitted curve (Trilinear curve)	$0\leq\theta_P<0.045$	$M_P=10.14\theta_P$	$-0.051\leq\theta_N<0$	$M_N=8.35\theta_N$
	$0.045\leq\theta_P<0.097$	$M_P=6.92\theta_P+0.15$	$-0.121\leq\theta_N<-0.051$	$M_N=3.01\theta_N-0.28$
	$\theta_P\geq0.097$	$M_P=0.82$	$\theta_N<-0.121$	$M_N=-0.64$

References

[1] Buitrago M., Moragues J.J., Calderón P.A. and Adam J.M., “Structural failures in cast-in-place reinforced concrete building structures under construction”, Handbook of Materials Failure Analysis, 6, 153–170, 2018.
[2] Beale R.G., “Scaffold research — a review”, Journal of Constructional Steel Research, 98, 188–200, 2014.
[3] Pieńko M. and Błazik-Borowa E., “Numerical analysis of load-bearing capacity of modular scaffolding nodes”, Engineering Structures, 48,1-9, 2013.
[4] Abdel-Jaber M., Beale R.G., Shatarat N.K. and Shehadeh M. A., “Experimental and theoretical investigations of spigot connections under cyclic loading”, Advanced Steel Construction, 15(1), 37-46, 2019.
[5] Cimellaro G.P. and Domaneschi M., “Stability analysis of different types of steel scaffolds”, Engineering structures, 152, 535-548, 2017.
[6] Chandrangsu T. and Rasmussen K.J.R., “Structural modelling of support scaffold systems”, Journal of Constructional Steel Research, 67(5), 866-875, 2011.
[7] Jia L., Liu H.B., Chen Z.H., Liu Y. and Wu Y.P., “Experimental study on bearing capacity

of reinforced steel tubular scaffold under uniform loads", Advances in Civil Engineering, 14, 1-20, 2019.
[8] Peng J.L., Wang S.H., Wang C.S. and Yang J.P., "Stability study on scaffolds with inclined surfaces and extended jack bases in construction", Advanced Steel Construction, 17(1), 73-83, 2021.
[9] Jia L., Liu H.B., Chen Z.H., Liu Q. and Wen S.L., "Mechanical properties of right-angle couplers in steel tube-coupler scaffolds", Journal of Constructional Steel Research, 125, 43-60, 2016.
[10] Abdel-Jaber M.S., Beale R.G., Godley M.H.R. and Abdel-Jaber M., "Rotational strength and stiffness of tubular scaffold connectors", Proceedings of the Institution of Civil Engineers Structures and Buildings, 162(6), 391-403, 2009.
[11] Abdel-Jaber M., Abdel-Jaber M.S., Beale R.G., Allouzi R. and Shatarat N.K., "Properties of tube and fitting scaffold connections under cyclical loads", Journal of Constructional Steel Research, 168, 106008, 2020.
[12] Prabhakaran U., Beale R.G. and Godley, M.H.R., "Analysis of scaffolds with connections containing looseness", Computers & Structures, 89, 1944-1955, 2011.
[13] Chandrangsu T. and Rasmussen K.J.R., "Investigation of geometric imperfections and joint stiffness of support scaffold systems", Journal of Constructional Steel Research, 67 (4), 576-584, 2011.
[14] Liu H.B., Zhou Y., Chen Z.H. and Liu, Q., "Structural performance and design method of new mortise-tenon full steel-tube scaffold", Advanced Steel Construction, 14(2), 291-307, 2018.
[15] Peng J.L., Wu C.W., Chan S.L. and Huang, C.H., "Experimental and numerical studies of practical system scaffolds", Journal of Constructional Steel Research, 91, 64-75, 2013.
[16] Bong J.K., Lee H.D., Kim S., Mha H.S., Yim D.K. and Won J.H., "Probabilistic characteristics of moment capacity and rotational stiffness of wedge joints used in support systems reflecting reused members", Applied Sciences, 9(19), 4056, 2019.
[17] Pieńko M. and Błazik-Borowa E., "Experimental studies of ringlock scaffolding joint", Journal of Constructional Steel Research, 173, 106265, 2020.
[18] Zhao Z.W., Liu H.Q., Dong J.F. and Bian Y.X., "Buckling Capacity of Socket-Template Scaffold System without X-Bracing", Journal of Performance of Constructed Facilities, 34(1), 04019089, 2020.
[19] Dong J. F., Liu H. Q., and Zhao Z. W., "Buckling behavior of a wheel coupler high-formwork support system based on semi-rigid connection joints", Advanced Steel Construction, 18(1), 425–435, 2022.
[20] Chen Z.H. and Zhao Z.W., "Analysis of door-type modular steel scaffolds based on a novel numerical method", Advanced Steel Construction, 12(3), 316-327, 2016.
[21] Liu C., He L., Wu Z.Y. and Yuan J., "Experimental study on joint stiffness with vision-based system and geometric imperfections of temporary member structure", Journal of Civil Engineering and Management, 24(1), 43-52, 2018.
[22] High strength sorbite stainless structural steel welded steel pipe: T/SSEA 0007-2017. Beijing: China special steel enterprises association, 2017.
[23] Temporary works equipment, Part 3: Load testing: EN 12811-3. London: British Standards Institute, 2002.
[24] The storage equipment manufacturers association: SEMA. London: UK Trade Association, 1985.
[25] Steel Static Storage Systems-Adjustable Pallet Racking Systems-Principles for Structural Design: EN 15512:2009. London: British Standards Institute, 2009.